

Reactive Flow in Supercritical Geothermal Settings and Its Impact on Electrical Fluid and Rock Properties

Juliane Kummerow, Siegfried Raab, Erik Spangenberg, Anja M. Schleicher and Jan Schüssler
GFZ German Research Centre for Geosciences, Telegrafenberg, 14473 Potsdam, Germany
jule@gfz-potsdam.de

Keywords: supercritical geothermal systems, electrical conductivity/resistivity, fluid-rock interactions

ABSTRACT

In recent years, the investigation of superheated/ supercritical hydrothermal systems linked to magmatic intrusions in volcanic environments became a more and more prominent target of geoscientific and engineering studies as the exploitation of reservoirs with fluid temperatures above 350 °C is expected to increase the energy output by up to a factor of ten. Deep resistivity surveys are regarded to provide a convenient means for detecting supercritical roots of geothermal reservoirs, as electrolytes, dissolved in aqueous solutions, have the tendency to associate at near- and supercritical conditions. The removal of charge carriers from the solution causes the reduction of fluid conductivity by an order of magnitude. However, mass transfer and diffusion-controlled chemical reactivity of aqueous solutions are enhanced at near- and supercritical conditions. In consequence, resistivity contrasts between sub- and supercritical systems may be blurred by fluid-rock interactions, what could reduce the spatial resolution of electrical measurements at field scale. Due to a lack in experimental data for the high-temperature range, in the framework of the European-Mexican GEMex project we have studied the impact of hydrothermal alteration processes on the electrical properties in reactive flow experiments under pressure and temperature conditions of unconventional high-enthalpy geothermal reservoirs ($T > 350$ °C, $p_{fluid} = 25$ MPa). We have tested water-rock systems of various lithologies (volcanic rocks, limestones) with different permeabilities. The measurements were supplemented by a number of additional tests, comprising microstructural investigations as well as the chemical analysis of fluid samples, after they percolated through the rocks at various temperatures.

1. INTRODUCTION

With the necessity for a reorientation of the power industry towards renewable energies on the one hand and the still high energy demand on the other, in recent magmatic areas the focus is increasingly on unconventional superheated and supercritical geothermal reservoirs. While conventional hydrothermal wells with bottom hole temperatures of 300 °C can yield up to 10 MWe, modeling studies indicate that the productivity of geothermal power plants might be enhanced to 40 – 50 MWe, when extracting superheated or supercritical fluids with temperatures of 430 – 550 °C (Albertsson et al., 2003, Fridleifsson and Elders, 2005). In the literature, the distinction between the terms “supercritical” and “superheated” is diffuse. Here, we use the term “supercritical” to describe a fluid phase at temperature and pressure conditions above the critical point, which is for pure water at 374 °C and 221 bar, whereby the critical point is shifted towards higher temperatures and pressures with increasing fluid salinity. With “superheated” we denote fluids at temperatures > 350 °C and pressure below 221 bar, whereby liquid and vapour phase coexist.

The identification of superheated or supercritical reservoirs for geothermal exploitation requires an accurate exploration of the target area by geophysical methods. For delineation of hydrothermal systems, particular cost-effective magneto-telluric surveys are suitable, as electrical properties are sensitive to temperature, porosity, fluid content and the nature of formation fluids in terms of phase and salinity. Several conduction mechanisms contribute in parallel to the electrical properties of a rock. Generally, electrolytic charge transport dominates in rocks saturated with pore fluids of moderate to high salinity, while at low fluid salinity, electrokinetic processes at the mineral-fluid interface becomes more important. Interface conductance is highly effective in the presence of minerals with high cation exchange capacity (CEC), such as clay minerals and zeolite (Flovenz et al., 1985). In contrast, intra-mineral electrical conductivity is of subordinate importance and becomes commonly relevant only in the presence of a sufficient amount of ore minerals. Moreover, all conduction mechanisms are temperature dependent. This is especially true for the electrolytic conduction through the pore fluid, which is governed by viscosity- and density-controlled changes in ion mobility, charge carrier density and di-electric number of the fluid (Quist and Marshall, 1968). All this makes the interpretation of electrical measurements very complex. Thus, the correlation between measurements at the earth surface and material properties at depth need for combined investigations on various scales. While field surveys and downhole measurements provide data on regional and local scale, petrophysical measurements at defined laboratory conditions can help to develop a more detailed understanding of the underlying processes on pore scale and are thus of utmost importance for the interpretation of field and logging data. However, due to the harsh experimental conditions, for temperatures above 250 °C petrophysical data on water-saturated rock samples are still limited, and for near-critical and supercritical conditions, both the experimental database as well as theoretical assumptions becomes even rarer. Glover and Vine (1992) studied the electrical conductivity (= inverse of resistivity) of low-porous, brine-saturated granulites, gneisses, amphibolites, granites, and diorite up to 200 MPa and 1000 °C. Due to the high content of sheeted silicates, the conductivity was found to be dominated by surface conductance. Ucock et al. (1980) have reported on resistivity measurements on porous sandstones up to 350 °C at 30 MPa confining pressure. They have used a high salinity fluid and found that the bulk conductivity displays a similar temperature dependence like the fluid conductivity, what points to the dominance of electrolytic conduction in their samples. Violay et al. (2012) and Nono et al. (2018) measured brine saturated volcanic rocks at a confining pressure of 100 MPa and temperatures up to 600 °C. The results of these measurements document that the electrolytic contribution to the bulk conductivity drastically decreases above 350 °C and becomes negligible at temperatures higher than 400 °C (Nono et al., 2018) as electrolytes tend to precipitate as salt from supercritical aqueous solutions (e.g. Quist and Marshall, 1968).

On the other hand, mass transfer and diffusion-controlled chemical reactions accelerate in supercritical electrolytic solutions, whereby the breakdown of minerals as well the formation of new ones changes the availability of charge carriers in the pore fluid. As none of the set-ups used so far, do offer the possibility of fluid flow, the effect of dynamic chemical conditions and the impact of high-temperature fluid-rock interactions on petrophysical parameters was not considered in measurements, yet. Here we present a study, dedicated to investigate the effect of mineral dissolution and/ or mineral precipitation on the bulk conductivity and water permeability of rocks, which were performed in long-term reactive flow experiments at pressure and temperature conditions of high-enthalpy geothermal reservoirs ($T > 300$ °C, $p_{fluid} > 22$ MPa). In the framework of the project GEMex the electrical and hydraulic conductivities of brine-saturated volcanic rocks and a limestone were investigated for increasing temperatures up to supercritical conditions to better understand fluid-driven processes in geological settings with a high heat flow.

2. EXPERIMENTAL SET-UP AND METHODOLOGY

Combined measurements of permeability and electrical conductivity of brine-saturated rock cores (30 mm in diameter and 75 mm in length) were conducted in an internally heated argon gas pressure chamber at a maximum confining pressure of 40 MPa and successively increasing temperatures ($T_{max} = 406$ °C). For permeability measurements, the sample set-up was connected to a pore pressure system, which was controlled by a pump each on up-stream and down-stream side. After the sample was led to equilibrate to the new temperature level for at least 6 hours, a certain flow rate was adjusted and kept constant for at least one hour until the differential pore pressure reached equilibrium. For permeabilities $< 10^{-19}$ m² it was more feasible to determine the flowrate, which adjusted for a given differential pressure between up-stream side and down-stream side. The electrical conductivity was determined from impedance logs, measured with a four-electrode layout (Zahner-Zennium Electrochemical Workstation). Details of the set-up and the measuring procedures are given in Kummerow and Raab (2015) and Kummerow et al. (2018).

When possible, fluid samples have been taken down-stream at every temperature level for chemical analysis with ICP-OES. In dependence of the permeability of the various rock samples flow rates ranged from 0.02 – 0.00002 ml/min. Therefore, for some experiments temperature levels had to be kept constant for several days to weeks to take a sufficient fluid volume. Occasionally, flow rates of less than 0.000002 ml/min arose. Here, no fluid samples could be taken at all.

3. SAMPLE MATERIAL

Geothermal systems with temperatures above 250 °C and a steep temperature gradient are usually associated with shallow magmatic intrusions in volcanic areas (Reinsch et al., 2017). Where the volcanic sequences rest on a sedimentary basement also these formations can be effected by hot geothermal systems, like in the Transmexican Volcanic Belt, where folded Cretaceous limestones and shales are part of the high temperature reservoir (Lopez-Hernandez et al., 2009). Hence, in this study hydraulic and electrical properties were determined both on volcanic rock samples (*KH5-09*, *GG1-qzDol*) and on a limestone (*15-AC-LC*). The mineral content and chemical composition of the pre- and post-experiments samples were determined by XRD measurements and Electron MicroProbe Analysis (EMPA). Initial and post-run sample porosities, ϕ , were defined at ambient conditions by the triple weight method on dry, saturated, and samples immersed in water (ISRM, 1981). The intrinsic electrical properties of the studied rock samples (formation factor, F , and interface conductance, σ_{if}) were determined at ambient conditions using the method described by Flovenz et al. (2005). The electrical tortuosity, τ , which is a measure for the pathlength of particle flow was calculated from $\tau = \sqrt{F \cdot \phi}$. The baseline parameters are summarised in Table 1.

Table 1: Baseline characterization of the studied rock cores and saturation fluids. Standard deviations are given.

sample number	GG1-qzDol	KH5-09	15-AC-LC
Lithology	quartz dolerite	volcanic breccia	limestone
porosity ϕ (%)	6.2 ± 0.02	30.7 ± 0.2	1.85 ± 0.08
formation factor, $F_{(ambient)}$	3300 ± 291	19.0 ± 0.3	515 ± 22
tortuosity, $\tau = \sqrt{F \cdot \phi}$	14.3	2.4	3.1
interface conductivity, $\sigma_{if (ambient)}$ (S m ⁻¹)	$7.8 \times 10^{-4} \pm 0.2 \times 10^{-4}$	$59.7 \times 10^{-4} \pm 0.4 \times 10^{-4}$	$0.4 \times 10^{-4} \pm 0.7 \times 10^{-6}$
pore fluid composition	NaCl – CaCl ₂ – K ₂ SO ₄	NaCl – CaCl ₂ – K ₂ SO ₄ – SiO ₂	0.1 M NaCl
pore fluid concentration (mol/L)	0.017	0.018	0.100
pore fluid conductivity $\sigma_{fl (ambient)}$ (S m ⁻¹)	0.228 ± 0.002	0.346 ± 0.002	1.016 ± 0.008

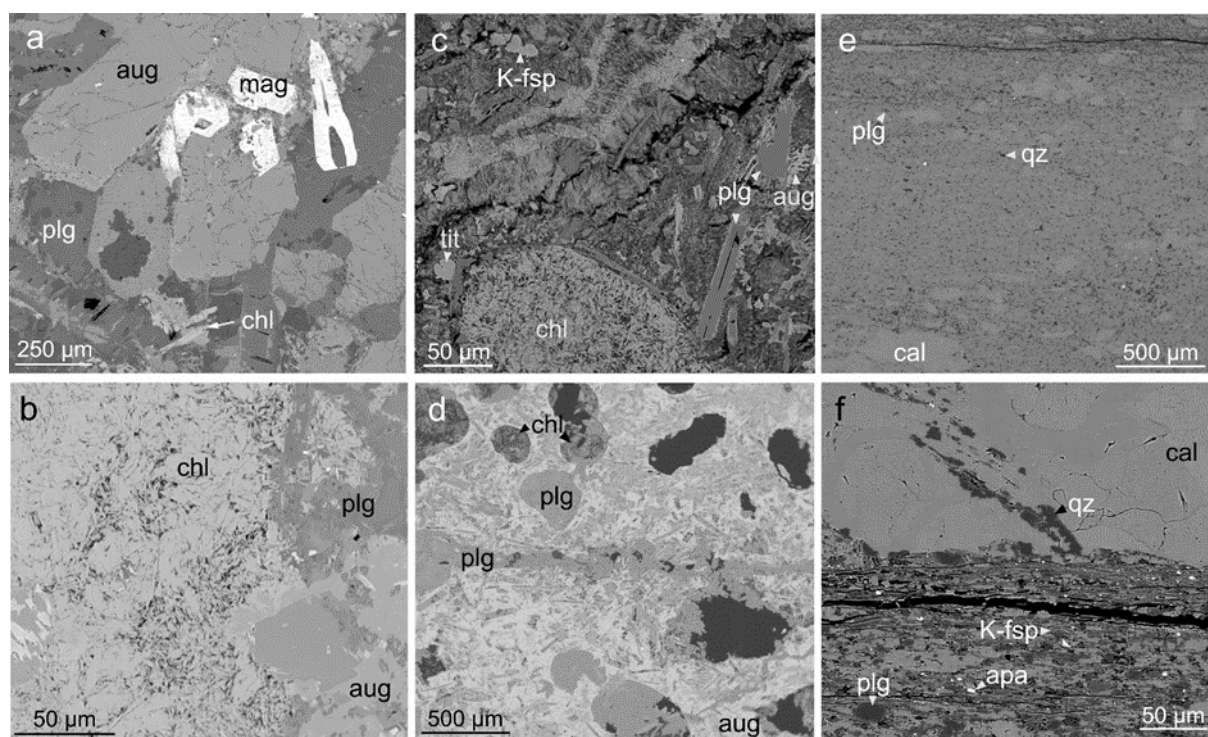


Figure 1: SEM images of the studied sample material. (a and b) quartz-dolerite GG1-qzDol, (c and d) volcanic breccia KH5-09, and (e and f) argillitic limestone 15-AC-LC. Abbreviations: aug = augite, chl = chlorite, mag = magnetite, plg = plagioclase, cal = calcite, k-fsp = K-feldspar, qz = quartz, apa = apatite.

Based on SEM and XRD analyses the mineral assemblage of the dolerite sample *GG1-qzDol* comprises plagioclase (44 %), augite (24 %), hornblende (14 %), chlorite (13 %), magnetite (3 %), and quartz (2 %). The porosity of 6.2 % is predominantly associated to randomly oriented fractures often lined with chlorite, while additional micropores were identified in larger chlorite aggregates (Figure 1a and b). Due to the low porosity the formation factor is very high ($F = 3382$). Despite the high amount of alteration minerals, the interface conductance at ambient conditions is low ($\sigma_{if} = 7.8 \mu\text{S/cm}$).

Sample *KH5-09* is classified as heterolithic volcanic breccia. It is highly altered and possesses a quite complex mineral paragenesis, comprising plagioclase (30 %), pyroxene (28 %), chlorite (15 %), orthoclase (13 %), quartz (8 %), calcite (2 %), actinolite (2 %), and epidote (1 %). It was chosen for its high porosity ($\phi = 30.7 \%$) at an acceptable permeability of $k = 9.01 \times 10^{-14} \text{ m}^2$ at ambient conditions. Both vesicular pores and cracks characterize the pore structure (Figure 1c and d). The breccia exhibits a formation factor of $F = 19.0$ and is characterised by an interface conduction of $\sigma_{if} = 59.7 \mu\text{S/cm}$.

Sample *15-AC-LC* is an argillitic limestone with intercalated sandy portions and consists of calcite (57 %), quartz (28 %), K-feldspar (8 %), albite (4 %), and the accessory minerals vesuvianite, rutile, apatite, and pyrite. *15-AC-LC* possesses only a minor initial effective porosity of 1.85 %, which is exclusively linked to open fissures along bedding planes (Figure 1e and f). For ambient conditions, a permeability of $5.63 \times 10^{-15} \text{ m}^2$ was determined. In consequence of the microstructure, the formation factor is high ($F = 515$). Predominantly due to the absence of sheeted silicates interface conductance is negligible ($\sigma_{if} = 0.4 \mu\text{S/cm}$).

As pore fluids for the volcanic samples we used diluted NaCl-dominated brines with a fluid conductivity of $\sigma_{fl} = 0.23 \text{ S/m}$ and $\sigma_{fl} = 0.35 \text{ S/m}$, respectively, at ambient conditions. For the limestone the pore fluid was a 0.1 M NaCl solution of intermediate conductivity ($\sigma_{fl} = 1 \text{ S/m}$). To minimize the oxygen content of the brines, they were degassed in a desiccator and then put permanently under nitrogen pressure to avoid corrosion of the flow through unit and the input of any impurities. During the flow-through experiments, fluid samples were collected at every temperature level and chemically analysed with ICP-OES to determine the concentrations, c_i , of the major cations ($i = \text{Na}^+, \text{K}^+, \text{Ca}^{2+}, \text{Si}^{4+}, \text{Al}^{3+}$) and anions ($i = \text{SO}_4^{4-}$) present in the studied fluid-rock systems.

4. RESULTS

4.1 Rock properties

Isobaric electrical resistivities/ conductivities and permeabilities of two volcanic rocks samples (*GG1-qzDol*, *KH5-09*) as well as of an argillitic limestone (*15-AC-LC*) were determined as function of temperature in long-term (up to 83 days) flow through experiments. The quartz-dolerite (*GG1-qzDol*) was measured two times, whereby temperatures of 350 °C and 300 °C were applied at maximum. Both runs had to be stopped after the set-up sustained a severe gas leakage at maximum temperature. However, the volcanic breccia as well as the limestone sample were exposed to supercritical conditions for about 4 and 8.5 hours, respectively. The results are plotted in Figure 2.

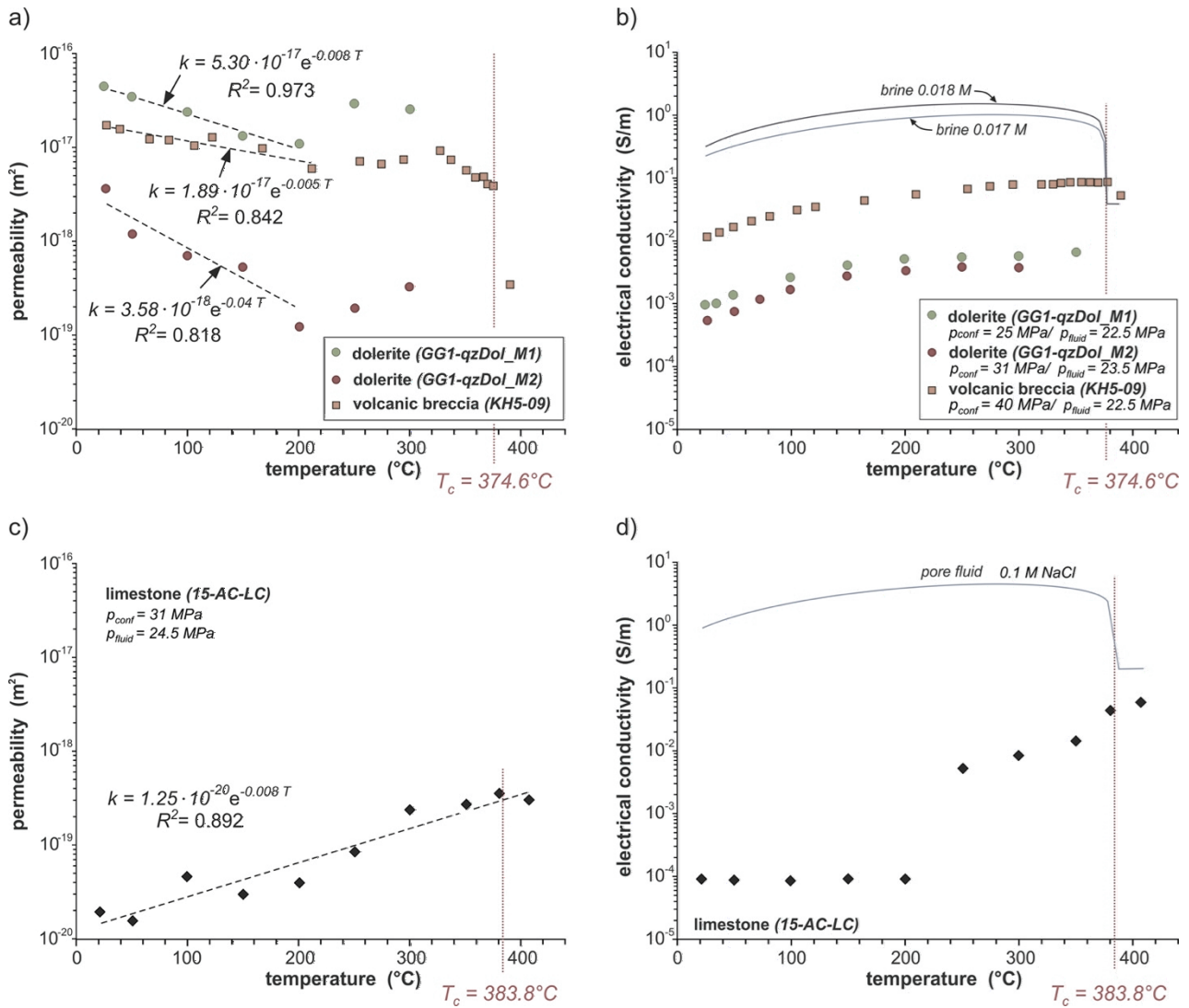


Figure 2: Permeabilities and electrical conductivities of fluid saturated volcanic rocks samples (a and b) and the limestone sample (c and d) as function of temperature. The volcanic rocks were saturated with diluted brines, whereas the limestone was saturated with 0.1 M NaCl solution. Fluid conductivities as function of temperature were measured in a separate flow-through cell (see Kummerow et al., 2018) and are plotted for comparison (blue lines). Dashed lines represent best-fit curves. Red dotted lines mark the critical temperature of the used fluids.

All rock samples are very sensitive to the confining pressure, what is expressed by a considerable reduction of permeability after the effective pressure was applied. This can be most probably attributed to a reduction of porosity due to sample compaction. Sample compaction is particularly effective for the parallelly fissured sample *15-AC-LC*, where the permeability, k , dropped by nearly four orders of magnitude from $5.63 \times 10^{-15} \text{ m}^2$ at ambient conditions to $6.13 \times 10^{-19} \text{ m}^2$, when a confining pressure of merely 1 MPa was applied, and to $1.95 \times 10^{-20} \text{ m}^2$ after setting the final confining pressure of 31.5 MPa. The permeability of the highly porous sample *KH5-09* decreased by about three orders of magnitudes. Here, we cannot exclude a reduction of effective permeability by a possible two-phase flow due to a marginal gas leakage. Experiments on the quartz-dolerite *GG1-qzDol* were run in two cycles (M1 and M2) at an effective pressure of 2.8 MPa and 7.5 – 8.5 MPa, respectively. For the higher confining pressure the permeability at 24 °C decreased by about 2 orders of magnitude compared to that at lower effective pressure (Figure 2a).

Generally, for the studied volcanic rocks up to 200 – 250 °C the permeabilities decrease exponentially. While for the volcanic breccia the permeability decrease of 65 % is moderately (from 1.7×10^{-17} to $6.0 \times 10^{-18} \text{ m}^2$), it is more pronounced for the dolerite, where the permeabilities in both runs decrease by 75 % and 95 %, from 4.5×10^{-17} to $1.1 \times 10^{-17} \text{ m}^2$ and from 3.6×10^{-18} to $2.0 \times 10^{-19} \text{ m}^2$, respectively. Above 250 °C, the permeabilities of the studied volcanic rocks increase significantly, before the decrease is continued at temperatures higher than 300 – 325 °C and culminates to a sudden drop in permeability by about 50 %, after the critical temperature is overstepped. In contrast to the permeability reduction, with increasing effective pressure at room temperature only a minor effect on the electrical conductivities, σ_{bulk} , of the volcanic rock samples is observed. In the first run of the dolerite ($p_{\text{eff}} = 2.8 \text{ MPa}$), σ_{bulk} raises linearly from $9.7 \times 10^{-4} \text{ S/m}$ (1034 Ωm) at room temperature to $5.3 \times 10^{-3} \text{ S/m}$ (189 Ωm) at 200 °C and up to $6.7 \times 10^{-3} \text{ S/m}$ (149 Ωm) at 350 °C. For the second run ($p_{\text{eff}} = 7.5 - 8.5 \text{ MPa}$), σ_{bulk} is $5.4 \times 10^{-4} \text{ S/m}$ (1862 Ωm) at room temperature, $3.2 \times 10^{-3} \text{ S/m}$ (363 Ωm) at 200 °C and raises to $3.9 \times 10^{-3} \text{ S/m}$ (268 Ωm) at 350 °C. For the highly porous hyaloclastite, σ_{bulk} is $1.2 \times 10^{-2} \text{ S/m}$ (86 Ωm) at room temperature, $4.5 \times 10^{-2} \text{ S/m}$ (18 Ωm) at 200 °C, and reaches nearly constant values of $8.7 \times 10^{-2} \text{ S/m}$ (11 Ωm) between 345 °C and the critical temperature of 374.6 °C.

For the parallelly fissured limestone, up to 200 °C almost no fluid flow was possible and the percolation rate through sample *15-AC-LC* was in a range of 10^{-5} to 10^{-6} ml/min, although up to 200 °C the differential pressure between up-stream and down-stream side was increased up to 6 MPa at an minimum effective pressure of 1 MPa to stimulate hydraulic fracturing. According to the low permeability of the sample, measured electrical resistivities are very high (k Ω m) and electrical properties of the limestone are presumably dominated by interface or mineral conductance instead of electrolytic conductivity. At 250 °C we assume thermally induced re-opening of the fissures and/ or cracking of the sample, as both permeability, k , and the electrical conductivity, σ_{bulk} , increase by 1 and 2 orders of magnitude, respectively. More specifically, the permeability raises from 3.9×10^{-20} m² at 200 °C to about 2.3×10^{-19} m² at 300 °C and 2.9×10^{-19} m² at 406 °C. The electrical conductivity soars from 9.1×10^{-5} S/m (~ 11 k Ω m) at 200 °C to 5.9×10^{-3} S/m (~ 169 Ω m) at 250 °C. At 406 °C (supercritical conditions), σ_{bulk} equilibrates at 5.9×10^{-2} S/m (17 Ω m).

4.2 Quenched fluids

To estimate the influence of fluid-rock interactions, fluid samples have been taken at every temperature step, (1) to control conductivity and the pH value of the percolated fluids, and (2) to chemically analyse them with ICP-OES. The results are plotted in Figure 3. The conductivity, σ_q , and pH of the quenched fluid samples were determined with commercial conductivity and pH sensors at room temperature and atmospheric pressure. For experiments *GG1-qzDol_M1* and *GG1-qzDol_M2* the conductivities and pH values of the quenched fluid samples are nearly constant for all temperature steps. Nonetheless, ICP-OES analysis reveals a slight increase in Si concentration in the quenched fluid samples with temperature. For experiment *15-AC-LC*, at subcritical conditions σ_q and pH values of all quenched fluid samples vary around their initial values. However, the fluid sample quenched from 406 °C (supercritical conditions) possesses a slightly increased conductivity by about 3 %, while the pH value increases significantly from 7.05 to 8.49. This is contrasted by the ICP-OES analyses, which show already for temperatures between 250 – 406 °C a distinct increase in both the concentration of Si and Ca. The largest impact on σ_q was found for experiment *KH5-09* (volcanic breccia), where the conductivity in the percolated fluid decreased significantly by 12 % after supercritical conditions were applied. This indicates a depletion of charge carriers, what is consistent with anhydrite precipitations found at the down-stream side of the sample (Figure 4). Nonetheless, despite the reduction of σ_q with temperature, the Si concentration in the percolated pore fluid samples successively increases at $T > 200$ °C.

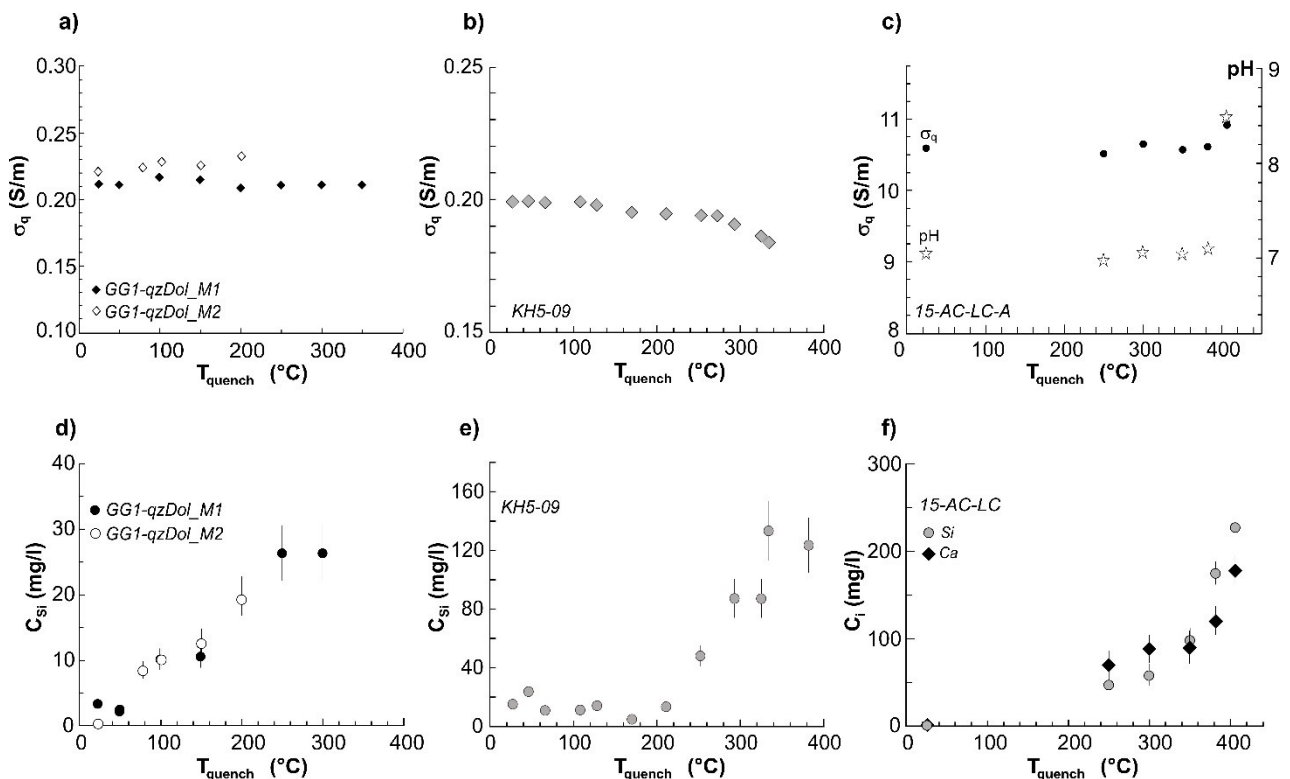


Figure 3: (a – c) Conductivities of quenched pore fluids, σ_q , percolated through the studied rock samples at various temperatures. Measurements at ambient conditions. (d – f) Si concentrations in the quenched fluids samples. Additionally, for the limestone sample, the Ca concentration is plotted. Fluid samples were taken at ambient conditions. Note that due to technical reasons for run *GG1-qzDol_M2* fluid samples could be taken just for temperatures up to 200 °C. In run *15-AC-LC*, in the temperature range between 50 – 200 °C, the collected fluid volume was insufficient for chemical analysis.

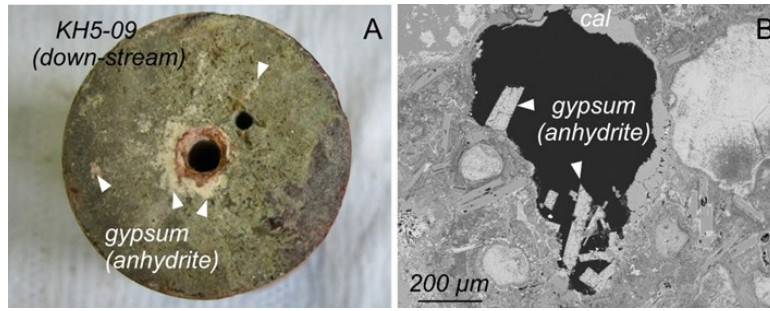


Figure 4: (A) Sample KH5-09 after finishing a high-temperature percolation experiment. The down-stream face is partially covered with gypsum minerals, which precipitated during the experiment as anhydrite. (B) SEM image from sample KH5-09 (post-run).

5. DISCUSSION

The hydraulic and electrical properties of a rock depend substantially on porosity, pore space structure (aspect ratio, connectivity), and the distribution of voids in the rock. All studied rock samples possess more or less pronounced crack-like pore networks. Such compliant or soft pores with low aspect ratios are largely affected by increasing effective pressure and temperature (Shapiro et al., 2015) and cause the observed substantial reduction in water permeabilities. The degeneration of the compliant crack networks of the dolerite and the volcanic breccia up to 200 °C seems not to affect their electrical properties, and σ_{bulk} and k are connected via power law relationships (Figure 5a and b). We assume that here hydraulic and electrical conductivity are related to different pore networks, whereby the electrical conductivity seems to be related to pores with a higher aspect ratio, which alter only slightly with increasing pressure and temperature and provide charge transport through the rock matrix, even at low water permeability. In contrast, the studied limestone sample exhibit no matrix porosity and the degradation of the fracture network is accompanied by a decline of both water permeability and electrical conductivity. Between 250 – 406 °C the permeability and electrical conductivity increase in a linear relation (Figure 5c), which also indicates that both transport properties are linked exclusively to the same fracture network.

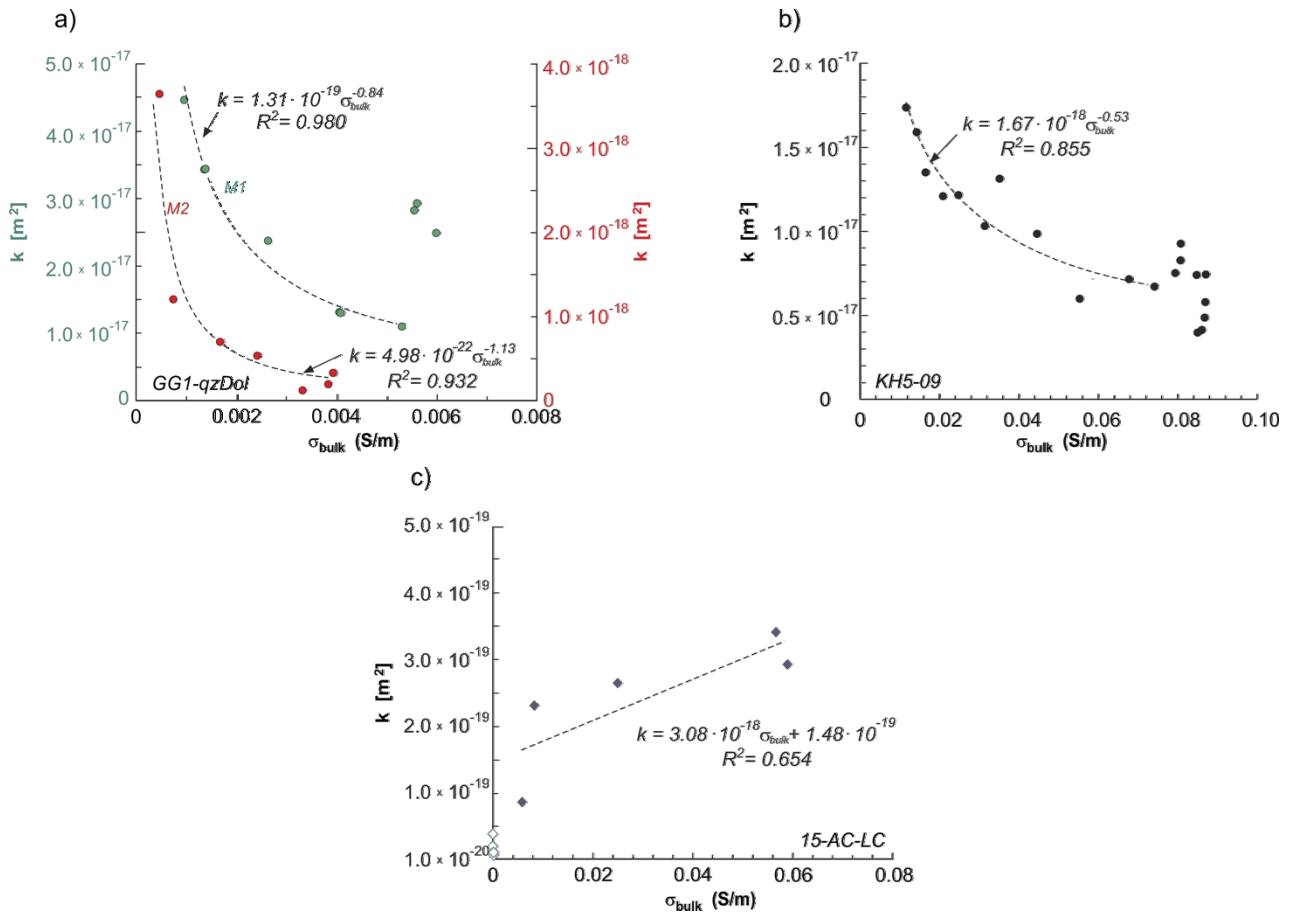


Figure 5: (a) Relationship of permeability, k , and bulk conductivity, σ_{bulk} , (a) for the studied dolerite (GG1-qzDol), (b) the volcanic breccia (KH5-09), and (c) for the limestone (15-AC-LC). Dashed lines are best-fit curves.

In fluid-saturated rocks, mainly composed of silicates or carbonates, the electrical bulk conductivity, σ_{bulk} , results primarily from ion mobility of the electrolytes in the pore space and from electrochemical interactions at the solid-fluid interface (Waxman and Smits, 1968; Schön, 1996). At fluid salinities > 1 S/m, the current transport is dominated by fluid conduction, σ_{fl} , and depends on the pore space structure (connectivity), which is represented by the formation factor, F , (e.g. Duba et al., 1978; Einaudi et al., 2005), that arise from Archie's relation (1942):

$$\sigma_{bulk} = \frac{\sigma_{fl}}{F} \quad (1)$$

It is established that the attachment of cations from the pore fluid to negatively charged mineral surfaces cause the formation of an electrical double layer at the mineral-fluid interface, the so-called surface or interface conduction, σ_{if} (Ruffet et al., 1995). Its contribution to σ_{bulk} depends on the porosity of the rock, the amount and distribution of minerals with high cation exchange capacity (clays, zeolites), and the fluid salinity (e.g. Patnode and Wyllie, 1950; Flovenz et al., 2005). Surface conductance becomes relevant for pore fluids with low salinity (< 1 S/m) and are often the dominating mechanism for current flow in rocks, saturated with highly diluted fluids of $\sigma_{fl} < 0.2$ S/m (Waxman and Smits, 1968; Revil and Glover, 1998; Nover, 2005). For crustal rocks containing only accessory ore minerals the conductivity through rock-forming minerals can be neglected, thus following the simplified relation of Waxman and Smits (1968) only σ_{fl} and σ_{if} act in parallel and the electrical bulk conductivity can be expressed then as (Rink and Schopper, 1976):

$$\sigma_{bulk} = \frac{\sigma_{fl}}{F^*} + \sigma_{if} \quad (2)$$

Fluid conductivity and interface conduction are governed by ion mobility and are thus highly temperature dependent. Up to 150 °C – 200 °C σ_{fl} and σ_{if} increase linearly, what can be written as

$$\sigma_{fl(T)} = \sigma_{fl(RT)} \left(1 + \alpha_{fl}(T - T_{RT}) \right) \quad (3)$$

and

$$\sigma_{if(T)} = \sigma_{if(RT)} \left(1 + \alpha_{if}(T - T_{RT}) \right), \quad (4)$$

respectively, with $\sigma_{fl(RT)}$ and $\sigma_{if(RT)}$ are the fluid and interface conductivities at room temperature and $\alpha_{fl}(T - T_{RT})$ and $\alpha_{if}(T - T_{RT})$ are the conductivity gradients for a distinct temperature range (Dakhnov, 1962; Flovenz et al., 1985). For electrolytic conduction through the pore space Dakhnov (1962) proposed a temperature gradient of $\alpha \approx 0.023$ °C⁻¹, whereas higher temperature gradients for conductivity of up to 0.040 ± 0.002 °C⁻¹ were observed for additional conduction along mineral – fluid interfaces (Sen and Goode, 1992; Revil and Glover, 1998). At temperatures above 200 °C, the effect of increasing ion mobility is counterbalanced by the expansion of the pore fluid, which causes an increasing reduction in the charge carrier density per unit volume. This effect is intensified near the critical point, when water loses its polar character and the solubility of inorganic salts decreases dramatically. In consequence, bulk conductivities decrease at temperatures higher than 300 °C (Nono et al., 2018). However, with temperature the chemical reactivity of aqueous solutions is enhanced and the dissolution or alteration of most rock-forming minerals accelerates. Increasing concentration of ions released to the pore fluid by mineral dissolution leads to increasing σ_{fl} . Hence, electrical bulk conductivity may also be affected by chemical fluid – rock interactions.

Based on the assumption that α is indicative for the underlying conduction mechanism, α_{bulk} was determined for the dolerite and the volcanic breccia and plotted together with α_{fl} of the used pore fluids in Figure 6a and c. Surface conductance is assumed to contribute to the bulk conductivity of the studied dolerite *GG1-qzDol* as $\alpha_{bulk} = 0.026$ °C⁻¹ compared to $\alpha_{fl} = 0.019$ °C⁻¹ is slightly increased. The contribution of σ_{if} is higher for the second run ($\alpha = 0.034$ °C⁻¹), indicating the influence of sample compaction and reduction of the width of flow paths on surface conduction. Between 250 – 300 °C, the pore fluid conductivity reaches maximum values that decrease sharply to the critical point at about 375 °C. This is due to a decrease in charge carriers per unit volume caused by the reduction in fluid density and dielectric number with temperature, which promotes the association of oppositely charged ions (Quist and Marshall, 1968; Kummerow et al., 2018). Accordingly, bulk conductivities related to ionic transport show a similar trend. Figure 6b shows the apparent formation factors, $F^* = \sigma_{fl} / \sigma_{bulk}$, which indicate that the increase in sample bulk conductivities with temperature is more pronounced than the observed conductivity increase of the pore fluids. For run *GG1-qzDol MI*, the trend is nearly linear throughout the studied temperature range and points to the dominance of increasing ionic mobility in the electrical double layer at the fluid-mineral interface. Compared to that, for the second test of the dolerite the decrease of F^* is steeper, but both trends become aligned at 150 °C. ICP-OES analyses of fluid samples revealed that the Si concentration in the pore fluid increased significantly by an order of magnitude with increasing temperature and indicates a beginning mineral dissolution at temperatures of about 200 °C. Nonetheless, due to the low permeability of the dolerite sample, the fluid – rock contact area was limited. Hence, absolute Si concentrations in the percolated fluid samples are low and probably the reason why no clear effect of fluid-rock interactions on bulk conductivities can be derived from the measurements.

In contrast, although the volcanic breccia *KH5-09* shows the highest interface conductance of all studied samples at ambient conditions, with increasing temperature σ_{bulk} is clearly dominated by σ_{fl} and only minor affected by σ_{if} , as both α_{fl} and α_{KH5-09} are nearly identical for temperatures up to 165 °C. This indicates that the pure proportion of minerals with pronounced CEC plays less of a role in surface conductivity processes under in-situ conditions than their distribution in the rock and its microstructural characteristics. At low temperatures, F^* values are in the range of the initial formation factor. Above 200 °C, the considerable steepening of the slope of the apparent formation factor points to the input of an extra conduction component and can be correlated to an increase in Si concentration of the pore fluid (see Figure 3). Between 330 °C and the critical point, σ_{bulk} becomes temperature-independent, at concomitant decrease in σ_{fl} . This strengthens the negative trend of F^* , which we attribute to the

precipitation of anhydrite (detected as gypsum in the thin section) from the pore fluid. The anhydrite precipitated in such a sufficient quantity that it was visible macroscopically at the end of the experiment (see Figure 4). Accordingly, we assume that partial clogging of fluid pathways gives rise to the observed drop in permeability of 60 % at supercritical conditions.

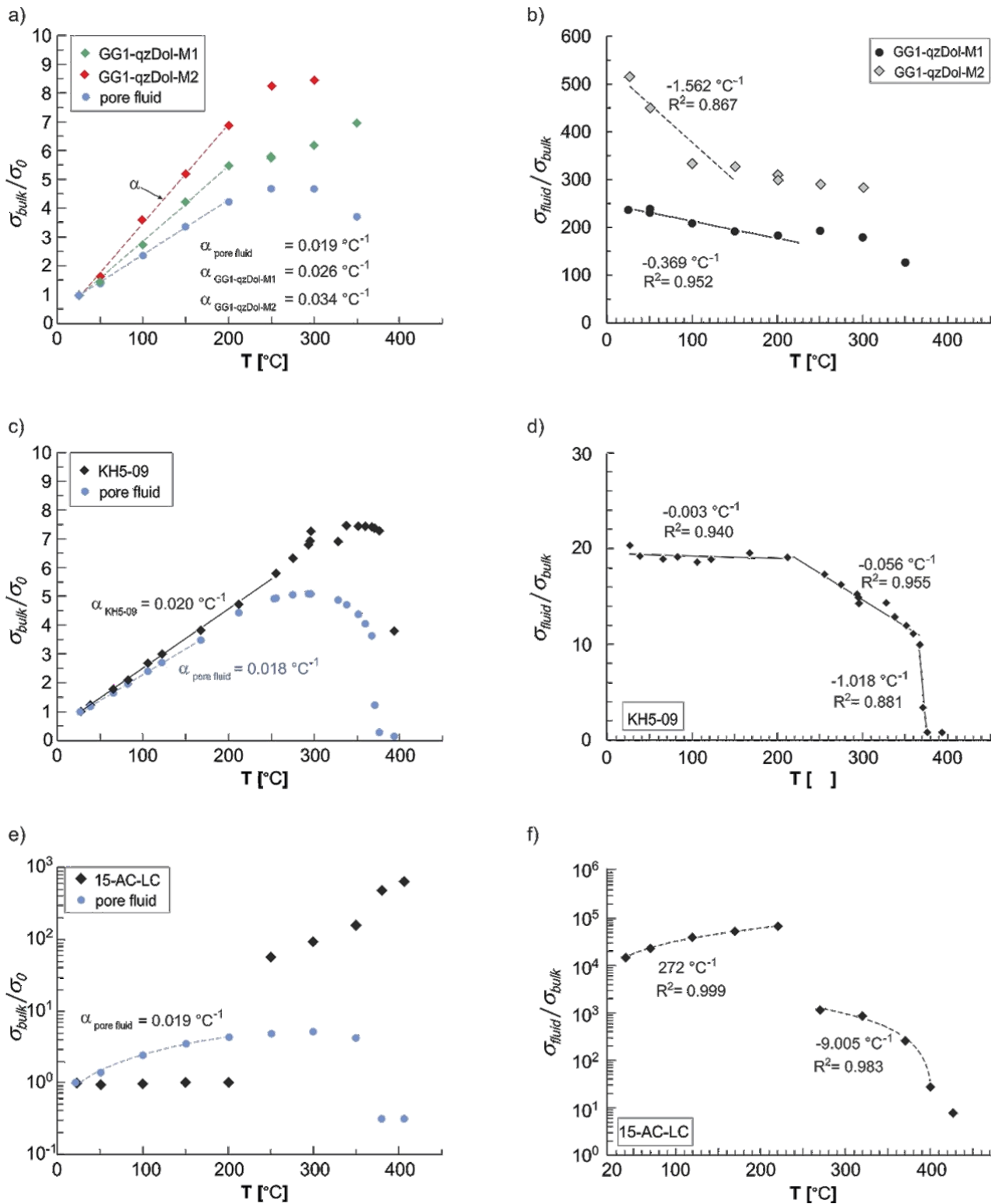


Figure 6: (a, c, e) Bulk electrical conductivities normalized on the conductivity at 24°C . The blue data sets represent normalized conductivities of the used pore fluids in dependence of temperature. Fluid conductivities were measured at corresponding temperatures in a separate flow-through cell (see Kummerow et al., 2018). The slope α represents the rate of conductivity increase for the temperature range $24 - 150^{\circ}\text{C}$. (b, d, f) The corresponding apparent formation factors were determined from fluid and bulk conductivities in dependence of temperature. Note that data in (e) and (f) are represented at log scale.

For the limestone sample *15-AC-LC*, two different conductivity mechanism can be derived from the trend of F^* : Due to the extensive sample compaction by applying the confining pressure and temperatures, up to 200 °C, σ_{bulk} varied only slightly around a nearly constant value of $9 \times 10^{-5} \text{ S m}^{-1}$, what corresponds to the initial surface conductance of the limestone. No temperature dependence was observed for this process. Accordingly, ionic charge transport is quite unlikely here. Revil and Glover (1998) proposed that surface conductivity is fed by three contributions: ionic charge transport both in the electrical diffuse layer and in the Stern layer, as well as proton or electron transfer in a thin layer on the mineral surface itself. Probably, the latter phenomenon was observed here. After the sample was thermally cracked at 250 °C, F^* dropped linearly, indicating that the conductivity mechanism changed and is most likely related to the flooding of the cracks with 0.1 M NaCl solution. Simultaneously with the onset of fluid transport through the sample, both the concentration of Si and Ca rapidly increase (see Figure 3f) and point to mineral dissolution along the flow paths. Consequently, the release of additional ions compensates the temperature-related negative density effect on ion concentration per fluid volume unit. Hence, here higher bulk conductivities arise, than expected for electrolyte conductance of an chemically inert system (Figure 6e) and σ_{bulk} raises exponentially up to supercritical conditions.

6. CONCLUSION AND SUMMARY

The electrical conductivity of electrolytic solutions is highly temperature sensitive, as ion mobility and charge carrier density are governed by changes in viscosity, density, and dielectric number of the fluid. In the past, electrical conductivity of brine-saturated rocks was found to show a similar temperature dependence, when charge transport through the rock was ion related, such as electrolytic and surface conductance: Up to 150 °C σ_{bulk} generally increase linearly, whereas the temperature dependence becomes less pronounced between 200 and 350 °C. Near the critical point, oppositely charged ions in electrolytes have the tendency to recombine. Thus, σ_{bulk} was found to become neglectable at supercritical conditions (Violay et al., 2012; Nono et al., 2018) and conductivity contrasts between sub- and supercritical systems are regarded to be significant to delineate geothermal high-enthalpy reservoirs. However, our study shows that fluid – rock interactions have the potential to mask these conductivity contrasts, as the concomitant entry of new charge carriers weakens the conductivity gradient in the near- and supercritical temperature range. The detectability of supercritical roots will mainly depend on the intensity of fluid-rock interactions, whereby its extent is a function of pressure, temperature, mineral compositions, exposure time and the specific surface area. Low permeable zones with less fluid–rock interactions might be characterized by a positive resistivity anomaly, while highly permeable areas with correspondingly extensive hydrothermal overprinting may be difficult to identify as supercritical, since high electrical conductivities due to a high load of charge carriers might lead to underestimated temperatures (Kummerow et al., 2018). Moreover, pronounced cleavage of a rock formation, as it is suspected for most high-enthalpy reservoirs, causes pronounced scale effects, and variations in the fluid-rock ratio, inner surface, pressure gradients, fracture orientation, etc. may considerably affect the mineral solubility and hence formation conductivities. Our experiments have shown that a parallel arrangement of cracks is more susceptible for pressure variations than a system containing randomly oriented cracks and the rate of fluid and charge transport is – in a crack-dominated environment - highly dependent on crack orientation and pore pressure.

ACKNOWLEDGEMENTS

We acknowledge the Comisión Federal de Electricidad (CFE) for kindly providing support and advice and for granting access to their geothermal fields. We are grateful to Helga Margret Helgadóttir, L. Weydt, K. Bär, C. Rochelle, B. Lepellier, D. Liotta, P. Deb for providing us with sample material. We are indebted to Ronny Giese and Mathias Kreplin for their invaluable support during the preparation of the experimental device. We also acknowledge our Icelandic and Mexican colleagues for their help and collaboration. The GEMex project has received funding from the EU in the framework of the Horizon 2020 research and innovation programme under the grant agreement no. 727550 and the Mexican Energy Sustainability Fund CONACYT-SENER, project 2015-04-68074. This study is a continuation of the FP 7 project IMAGE – Integrated Methods for Advanced Geothermal Exploration (grant agreement no. 608553).

REFERENCES

- Albertsson, A., Bjarnason, J.Ö., Gunnarsson, T., Ballzus, C., and Ingason, K.: The Iceland Deep Drilling Project: Fluid Handling, Evaluation and Utilization. International Geothermal Conference, Reykjavik, September 2003; 23-29.
- Archie, G.E.: The electrical resistivity log as an aid in determining some reservoir characteristics. *Petrol. Trans.*, **AIME 146**, (1942), 54-62.
- Arnórsson, S., Axelsson, G., and Sæmundsson, K.: Geothermal systems in Iceland: Jökull. *Icelandic Journal of Earth Sciences*, **58**, (2008), 269–302.
- Bingley, A., Slater, L.D., Fukes, M., and Cassiani, G.: Relationship between spectral induced polarization and hydraulic properties of saturated and unsaturated sandstone. *Water Resources Res.*, **41**, (2005), W12417, DOI: 10.1029/2005WR004202.
- Browne, P.R.L., and Ellis, A.J.: The Ohaki-Broadlands hydrothermal area, New Zealand: mineralogy and related geochemistry. *Am J Sci*, **269**, (1970), 97-131.
- Dakhnov, V.N.: Geophysical well logging: The application of geophysical methods; electrical well logging. *Q. Colo. Sch. Mines*, **57** (2), (1962), 445 pp.
- Driesner, T., and Heinrich, C.A.: The system H₂O–NaCl. Part I: Correlation formulae for phase relations in temperature–pressure–composition space from 0 to 1000 °C, 0 to 5000 bar, and 0 to 1 X_{NaCl}. *Geochim Cosmochim Acta*, **71**, (2007), 4880-4901.
- Duba, A., Piwinski, A.J., Santor, M, Weed, H.C.: The electrical conductivity of sandstone, limestone and granite. *Geophys. J. R. Astron. Soc.*, **53**, (1978), 583-597.
- Duba, A., Roberts, and J., Bonner, B.: Electrical properties of geothermal reservoir rocks as indicators of porosity distribution. *Proceedings 1997, 22th Workshop on Geothermal Reservoir Engineering Stanford University, Stanford, California, January 27-29, (1997), SGP-TR-155.*

- Einaudi, F., Pezard, P.A., Ildefonse, B., and Glover, P.: Electrical properties of slow-spreading ridge gabbros from ODP hole 1105A, SW Indian Ridge. In: Havey PK, Brewer TS, Pezard PA, Petrov VA, editors. Petrophysical properties of crystalline rocks. Geol. Soc London Spec Pub, **240**, (2005).
- Ewers, G.R.: Experimental hot water-rock interactions and their significance to natural hydrothermal systems in New Zealand. *Geochem Cosmochem Acta*, **41**, (1971), 143-150.
- Flovenz, O.G., Spangenberg, E., Kuhlenskampff, J., Arnason, K., Karlsdottir, R., Huenges, E.: The role of electrical interface conduction in geothermal exploration. Proceedings World Geothermal Congress 2005, Antalya, Turkey, 24-29 April 2005.
- Fridleifsson, G.O., and Elders, W.A.: The Iceland Deep Drilling Project: a search for deep unconventional geothermal resources. *Geothermics*, **34**, (2005), 269-285.
- Fuji-ta, K., Katsura, T., Ichiki, M., Matsuzaki, T., and Kobayashi, T.: Variations in electrical conductivity of rocks above metamorphic conditions, *Tectonophysics*, **504 (1-4)**, (2011) 116-121.
- Glover, P.W.J., and Vine, F.J.: Electrical conductivity of carbonbearing granulite at raised temperatures and pressures. *Nature*, **360**, (1992), DOI: 10.1038/360723a0.
- Glover, P.W., Ross, R.G., and Jolly, H.: The measurement of saturated rock electrical conductivity at lower crustal temperatures and high pressures. *High Press Res*, **5**, (1990), 705-707.
- ISRM Suggested Methods – Rock characterization testing and monitoring, Ed. E.T. Brown, published for the commission on testing methods, International Society for Rock Mechanics, published by Pergamon Press 1981, 210 pp.
- Izquierdo, G., Arellano, V.M., Aragón, A., Portugal, E., and Martínez, I.: Fluid acidity and hydrothermal alteration at the Los Huecos geothermal reservoir Puebla, Mexico. Proc. World Geotherm. Congress 2000, Kyushu-Tohoku, Japan, May 28 – June 10, (2000), 1301-1306.
- Milsch, H., Kristinsdottir, L.H., Spangenberg, E., Bruhn, D., and Flovenz, O.G.: Effect of the water-steam phase transition on the electrical conductivity of porous rocks, *Geothermics*, **39 (1)**, (2010), 106-114.
- Kulenkampff, J., Spangenberg, E., Flovenz, O., Raab, S., and Huenges, E.: Petrophysical Parameters of Rocks Saturated with Liquid Water at High Temperature Geothermal Reservoir Conditions. Proceedings, World Geothermal Congress 2005, Antalya, Turkey, 24-29 April 2005.
- Kummerow, J., Raab, S., Schuessler, J. A., and Meyer, R.: Non-reactive and reactive experiments to determine the electrical conductivities of aqueous geothermal solutions up to supercritical conditions. – J. Vol. Geotherm. Res., (2018 online first), DOI: 10.1016/j.volgeo.2018.05.014.
- Kummerow, J., and Raab, S.: Temperature dependence of electrical resistivity—Part II: a new experimental set-up to study fluid-saturated rocks. Energy Procedia*, **76**, (2015), 247–255, doi: 10.1016/j.egypro.2015.07.855.
- Lacinska, A.M., Rochell, C.A., and Kemp, S.J.: Petrographic description of a hydrothermally-altered andesite from well H-48, depth 1038 m, Los Humeros, Mexico, Brit. Geol. Survey External Report, CR/18/108, (2018), 37 pp.
- Lemmon, E.W., McLinden, M.O., and Friend, D.G.: Thermophysical Properties of Fluid Systems. In: Linstrom PJ, Mallard WG, editors. NIST Chemistry WebBook, NIST Standard Reference Database Number 69, (2005), National Institute of Standards and Technology, Gaithersburg MD, 20899 (<http://webbook.nist.gov>).
- Llera, F.J., Sato, M., Nakatsuka, K., and Yokoyama, H.: Temperature dependence of the electrical resistivity of water-saturated rocks, *Geophysics*, **55**, (1990), 576-585.
- López-Hernández, A., García-Estrada, G., Aguirre-Díaz, G., González-Partida, E., Palma-Guzmán, H., and Quijano-León, J.L.: Hydrothermal activity in the Tulancingo-Acocolco Caldera Complex, central Mexico: Exploration studies. *Geothermics*, **38**, (2009), 279-293.
- Nono, F., Gibert, B., Parat, F., Loggia, D., Cichy, S.B., and Violay, M. Electrical conductivity of Icelandic deep geothermal reservoirs up to supercritical conditions: Insight from laboratory experiments. J. Vol. Geoth. Res., (online first 2018), DOI: 10.1016/j.volgeo.2018.04.021.
- Nover, G.: Electrical properties of crustal and mantle rocks – a review of laboratory measurements and their explanation. *Surveys in Geophysics*, **26**, (2005), 593–651.
- Patnode, H.W., and Wyllie, M.R.J.: The presence of conductive solids in reservoir rocks as factor in electric log interpretation. *Petrol Trans, AIME* **189**, (1950), 47-52.
- Reinsch, T., Dobson, P., Asanuma, H., Huenges, E., Poletto, F., and Sanjuan, B.: Utilizing supercritical geothermal systems: a review of past ventures and ongoing research activities, *Geotherm Energy*, **5 (16)**, (2017), DOI 10.1186/s40517-017-0075-y.
- Revil, A., and Glover, P.W.J.: Nature of surface electrical conductivity in natural sands, sandstones, and clay. *Geophys. Res. Lett.*, **25 (5)**, (1998), 691-694.
- Revil, A., Cathles III., L.M., Losh, S., and Nunn, J.A.: Electrical conductivity in shaly sands with geophysical applications. *J. Geophys. Res.*, **103**, (1998), 23925-23936.
- Rink, M., and Schopper, J.R.: pore structure and physical properties in porous sedimentary rocks. *Pure Appl. Geophys.*, **114**, (1976), 273-284.
- Shapiro, S.A.: Elastic piezosenitivity of porous and fractured rocks. *Geophysics*, **68 (2)**, (2003), 482-486.

- Shapiro, S.A., Khizhniak, G.P., Plotnikov, V.V., Niemann, R., Ilyushin, P.Yu., and Galkin, S.V.: Permeability dependency on stiff and compliant porosities: a model and some experimental examples; *J Geophys Eng*, **12** (3), (2015), 376-385, doi:10.1088/1742-2132/12/3/376.
- Ucok, H.: Temperature Dependence of the Electrical Resistivity of Aqueous Salt Solutions and Solution Saturated Porous Rocks, *Ph.D. Dissertation, University of Southern California*. Quist, (1979).
- Ucok, H., Ershaghi, I., and Olhoeft, G.R.: Electrical resistivity of Geothermal Brines. *J Petrol Technol*, **32** (4), (1980), 717 – 727.
- Violay, M., Gibert, B., Azais, P., Lods, G., Pezard, P.A.: A new cell for electrical conductivity measurements on saturated samples at upper crustal conditions. *Transp. Porous Media*, **91**, (2012), 303-318, DOI: 10.1007/s11242-011-9846.
- Waxman, M.H., and Smits, L.J.M.: Electrical conductivities in oil-bearing shaly sands. *J Soc Petrol Eng*, **8**, (1968), 107-122.
- Zimmerman, R.W., Somerton, W.H., and King, M.S.: Compressibility of porous rocks. *J Geophys Res*, **91**, (1986), 12765-12777.